Journal of Prevention, Diagnosis and Management of Human Diseases
Vol: 06, No. 02, July-Dec 2026
ISSN: 2799-1202, DOI: 10.55529/jpdmhd.62.33.42

Research Paper

Quantifying COVID-19 pneumonia severity on chest radiographs: Automated lung density, radiologist scores, clinical outcomes and the confounding role of image acquisition

Astanov Shavkatbek[1*], Chaulagain Dipak[2], Orozbaeva Zhyldyzkan[3]
[1*]Department of Clinical Disciplines, Jalal-Abad International University, 720906, 24 Kurmanbek Str., Manas, Kyrgyzstan.
[2]Department of Clinical Disciplines, Jalal-Abad International University, 720906, 24 Kurmanbek Str., Manas, Kyrgyzstan.
[3]Department of Natural and Humanities Disciplines, Jalal-Abad International University, 720906, 24 Kurmanbek Str., Manas, Kyrgyzstan.

Article Info

Article History:
Received: 22 March 2026
Revised: 01 June 2026
Accepted: 08 June 2026
Published: 26 July 2026

Keywords:
COVID-19
Chest Radiography
Pneumonia Severity
Lung Segmentation
Prognosis
Intensive Care

ABSTRACT

Background: Chest radiograph severity scores aid triage of viral pneumonia, and automated scoring could support overstretched services.
Objective: To evaluate a transparent, segmentation-based severity measure on a public multi-source COVID-19 image collection.
Methods: Of 782 frontal radiographs from 449 patients, 93 had radiologist extent (0-8) and opacity (0-6) scores, and outcomes were available for up to 118 patients. A U-Net trained on an independent tuberculosis dataset (Montgomery County, 138 images) segmented aerated lungs. Relative lung density (RLD; ratio of lung to median body intensity) and zone-wise densities were computed.
Results: RLD correlated moderately with extent (Spearman rho = 0.59, 95% CI 0.40-0.74) and opacity (rho = 0.55) scores. A cross-validated zone model predicted extent (rho = 0.62; mean absolute error 1.52 vs. 2.01 for the mean). Middle-zone densities were the most informative (rho = 0.56-0.63). Segmentation transferred imperfectly: median Dice versus lungVAE reference masks was 0.89, but in 26% of native radiographs from one hospital, mostly intensive care images, less than 10% of the image was recognised as lung because consolidated lung was excluded. RLD on the first radiograph predicted death (AUROC 0.72, 95% CI 0.57-0.86), similar to age (0.73), but not ICU admission (0.56). Projection alone (anteroposterior vs. posteroanterior) predicted ICU admission (AUROC 0.74, 95% CI 0.66-0.82). Intensive care admission occurred in 67-88% of AP-imaged patients versus 12-35% of PA-imaged patients.
Conclusion: Automated lung density captures part of radiologist-assessed severity. In public COVID-19 collections, however,

Journal of Prevention, Diagnosis and Management of Human Diseases (JPDMHD)

acquisition factors are strong proxies for outcome. Prognostic models must adjust for projection and setting, and segmentation must be validated in severely opacified lungs before clinical use.

Corresponding Author:
Astanov Shavkatbek
Department of Clinical Disciplines, Jalal-Abad International University, 720906, 24 Kurmanbek Str., Manas, Kyrgyzstan
Email: astanovshavkat697@gmail.com

Copyright © 2026 The Author(s). This is an open access article distributed under the Creative Commons Attribution License, (http://creativecommons.org/licenses/by/4.0/) which permits unrestricted use, distribution, and reproduction in any medium, provided the original work is properly cited.

1. INTRODUCTION

Chest radiography is the most widely available imaging test for patients with pneumonia, and during the COVID-19 pandemic it was used to assess disease extent, triage patients and monitor progression [1]. Semi-quantitative severity scores, which grade the extent and density of opacities in each lung, are associated with oxygen requirement, intensive care admission and death [2], [3], [4], [5]. Their manual application, however, is time-consuming and subject to inter-reader variation, which has motivated automated scoring [6].

Most automated approaches to COVID-19 imaging have been developed on public image collections assembled from heterogeneous sources, and systematic reviews have found that nearly all published models were at high risk of bias [7], [8]. Models can exploit shortcuts such as hospital-specific markers, patient positioning or the projection used, rather than lung pathology [9], [10]. Patients who are too ill to stand are imaged supine in anteroposterior (AP) projection, often in the intensive care unit (ICU), whereas ambulatory patients are imaged posteroanterior (PA). Any image-derived prognostic model can therefore learn the setting rather than the disease.

This study examines these issues with a transparent pipeline rather than a black-box classifier. Using real radiographs from the public COVID-19 image data collection [11], it (i) assesses how a lung segmentation model trained on an independent dataset transfers to COVID-19 radiographs; (ii) evaluates an automated relative lung density measure against radiologist severity scores; (iii) tests its association with ICU admission, intubation and death; and (iv) quantifies how strongly the radiographic projection itself predicts these outcomes.

2. METHODOLOGY

2.1 Data

The COVID-19 image data collection [11], [12] contains radiographs and CT images gathered from publications, websites and hospitals, with metadata on diagnosis, projection, age, sex, days since symptom onset or admission, and outcomes (ICU admission, intubation and survival at any time during the illness). All 782 frontal radiographs (PA, AP, AP supine and AP erect) from 449 patients were included; 478 images from 295 patients were labelled COVID-19. For 93 COVID-19 radiographs from 64 patients, the collection provides severity scores averaged over three expert raters [6]: the geographic extent of ground-glass opacity or consolidation (0–4 per lung, total 0–8) and the degree of opacity (0–3 per lung, total 0–6). Of these, 82 were PA, 8 AP and 3 AP supine; patients were 25–84 years old (median 60). For outcome analyses, the first COVID-19 radiograph of each patient was used. A subset of 164 images from 71 patients originates from the Hannover Medical School repository of native clinical radiographs, released under a CC BY 3.0

licence [13]. Because many other images carry non-commercial licences or none, all radiographs reproduced in the figures of this article were taken from this openly licensed subset. The images are anonymised and publicly released.

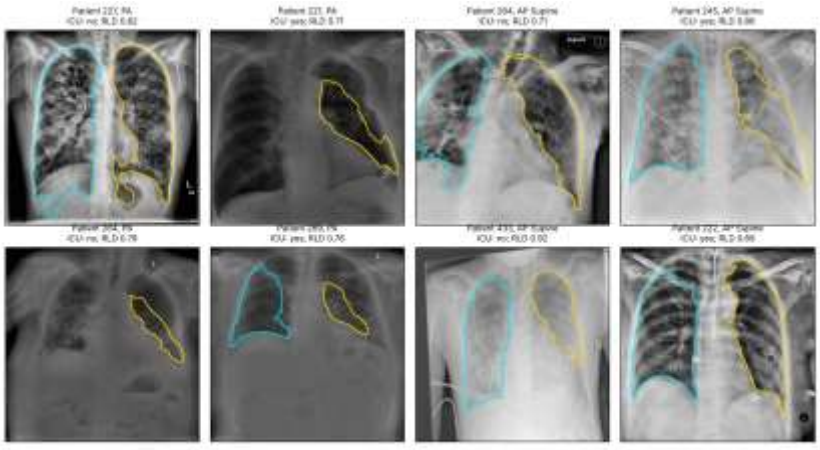

Figure 1. Real Radiographs of COVID-19 Patients from the Hannover Medical School Subset (CC BY 3.0) [13], Two per Combination of Projection (PA, AP Supine) and ICU Admission, with the Automatic Lung Masks (Cyan: Patient's Right Lung; Yellow: Left) and the Relative Lung Density (RLD). Note the Tubes, Lines and Electrodes in Supine ICU Images and the Incomplete Masks in Opacified or Low-Contrast Lungs.

2.2 Lung Segmentation

A compact U-Net [14] (five levels, 8–96 channels) was trained on all 138 radiographs of the NLM Montgomery County set with expert lung masks [15], [16], at 256 × 256 pixels, for 45 epochs with a combined cross-entropy and Dice loss and augmentation by rotation (±10°), scaling (0.85–1.15), translation, gamma, contrast and noise. It was then applied without further training to all 782 COVID-collection radiographs; the two largest components were kept, assigned to the right or left lung and hole-filled. Because no manual masks are available for the collection, agreement was measured against the lung masks provided with it for 199 frontal images, which were generated by a variational imputation model designed to include opacified lung (lungVAE) [17]. The fraction of the image recognised as lung was recorded as an additional quality indicator; the mean in the Montgomery training data was 25.5%.

2.3 Relative Lung Density

Because the images come from many sources with different exposure and post-processing, absolute intensities are not comparable. Each image was therefore normalised by the median intensity of the body (pixels above the 5th intensity percentile), and the relative lung density (RLD) was defined as the mean normalised intensity within the segmented lungs. Opacities raise the intensity of aerated lung towards that of soft tissue, so RLD increases with disease. Four reference normalisations were compared on the scored images, and the median-body reference, which gave the highest correlation, was retained; this choice was made on the same data and is a source of optimism. RLD was also computed separately for the upper, middle and lower thirds of each lung, and the fraction of each lung's convex hull not covered by the mask (lost aeration), the hull area and the lung area were recorded.

2.4 Statistical Analysis

Agreement of RLD with radiologist scores was measured by Spearman's ρ with 95% confidence intervals from a bootstrap that resampled patients. A ridge regression model ($\alpha = 10$) on the 10 zone and shape features was evaluated with leave-one-patient-out cross-validation to predict each score; mean absolute error, bias and Bland–Altman limits of agreement [18] were reported. For outcomes, the AUROC of RLD, age and projection (AP vs. PA; supine vs. not) was computed on the first radiograph of each patient, with bootstrap confidence intervals, and cross-validated logistic models combining RLD with projection or

age were fitted [19], [20]. Analyses were repeated within the single-centre Hannover subset and within projection strata. Reporting follows the relevant items of the TRIPOD statement [21].

3. RESULTS AND DISCUSSION

3.1 Transfer of Lung Segmentation

Applied to the COVID-19 collection, the U-Net found both lungs in 94.5% of radiographs. Agreement with the lungVAE reference masks had a median Dice coefficient of 0.89 (interquartile range 0.82–0.93; n = 199), with 18 images below 0.70 Figure 2. Segmentation failures had two causes. First, the network, trained on largely normal and tuberculosis radiographs, excluded densely consolidated lung, so that in severe cases only the remaining aerated lung was outlined Figure *1* and Figure *6*. Second, some low-contrast or heavily processed images were poorly segmented even when disease was moderate Figure 2. Less than 10% of the image was recognised as lung in 8.1% of all radiographs, in 12.4% of AP supine images and in 26.2% of the native Hannover images, most of which were ICU radiographs.



Figure 2. Transfer of the Montgomery-Trained U-Net to Real COVID-19 Radiographs (Hannover Subset): Images with the Smallest and an Intermediate and Large Recognised Lung Area, and the Distribution of Dice Agreement with the lungVAE Masks Supplied with the Collection (Right)

3.2 Agreement with Radiologist Severity Scores

Figure 3 shows relative density maps of real radiographs with increasing RLD. Across the 93 scored images, RLD correlated with the radiologist extent score (ρ = 0.59, 95% CI 0.40–0.74) and opacity score (ρ = 0.55, 0.35–0.70); within PA images only, the correlation with extent was 0.54 (not tabulated; Table 1 and Figure 4). The cross-validated zone model performed slightly better, with ρ = 0.62 (0.45–0.75) for extent and 0.59 (0.41–0.74) for opacity. Its mean absolute error was 1.52 points on the 0–8 extent scale and 0.98 points on the 0–6 opacity scale, compared with 2.01 and 1.25 points for predicting the mean score for every image, and the 95% limits of agreement were ±3.5 and ±2.3 points. Middle-zone densities correlated most strongly with extent (right 0.63, left 0.56), followed by the right upper zone (0.43; not tabulated); lower-zone densities, which overlap the diaphragm and heart, were weaker (0.24–0.33). Lost aeration and lung area alone correlated only weakly (|ρ| ≤ 0.17).

Table 1. Agreement Between Automated Measures and Radiologist Severity Scores (93 Radiographs, 64 Patients). Confidence Intervals from a Patient-Level Bootstrap; the Zone Model Was Evaluated with Leave-One-Patient-Out Cross-Validation

Automated Measure	Extent Score (0–8): ρ (95% CI)	Opacity Score (0–6): ρ (95% CI)	MAE Extent / Opacity	Limits of Agreement Extent / Opacity
Relative lung density (RLD)	0.59 (0.40–0.74)	0.55 (0.35–0.70)	—	—
Zone model (ridge, 10 features)	0.62 (0.45–0.75)	0.59 (0.41–0.74)	1.52 / 0.98	±3.5 / ±2.3

Predicting the mean score	—	—	2.01 / 1.25	—
Right / left middle-zone density	0.63 / 0.56	0.59 / 0.51	—	—
Right / left lower-zone density	0.33 / 0.24	0.34 / 0.31	—	—
Lost aeration, right / left lung	−0.12 / −0.12	−0.17 / −0.14	—	—

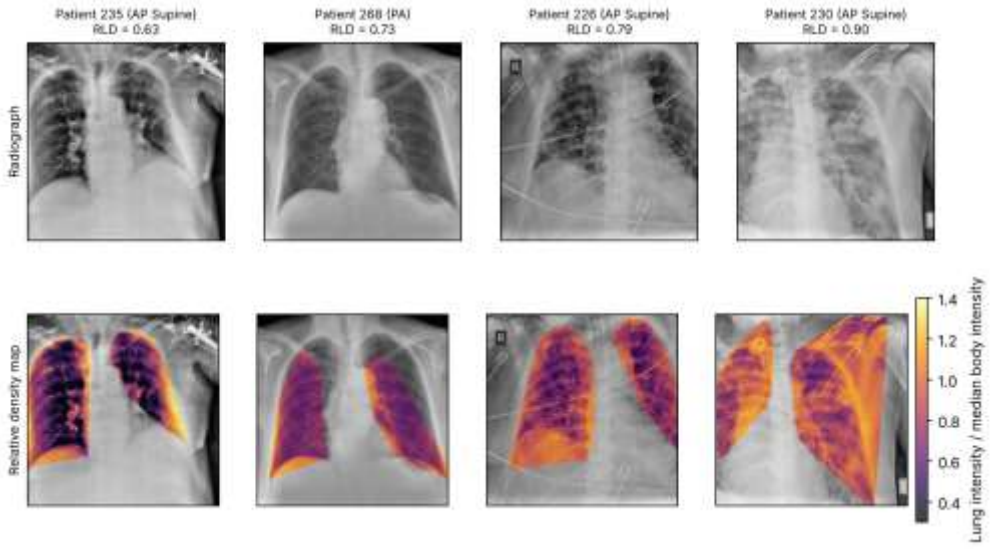

Figure 3. Real Radiographs from the Hannover Subset with Increasing Relative Lung Density (Top) and the Corresponding Relative Density Maps within the Convex Hull of Each Lung (Bottom; Lung Intensity Divided by the Median Body Intensity)

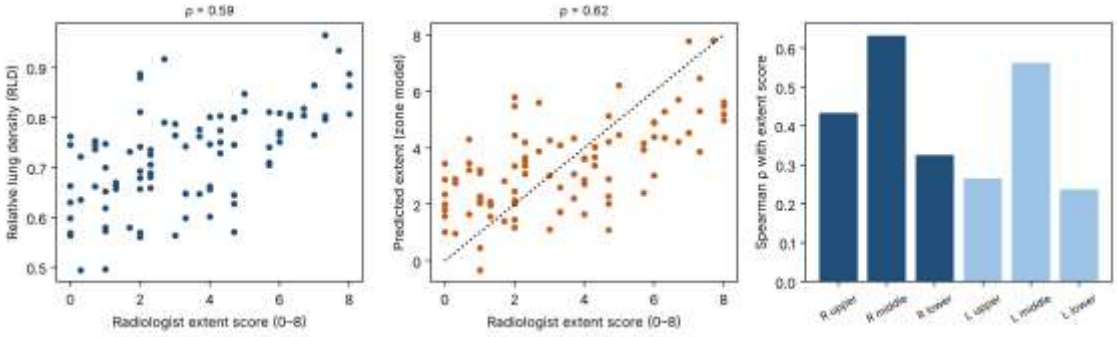

Figure 4. Agreement with Radiologist Severity Scores: Relative Lung Density (Left) and the Cross-Validated Zone-Model Prediction (Centre) Against the Radiologist Extent Score, and the Correlation of Each Lung Zone's Density with the Extent Score (Right).

3.3 Outcomes and the Role of Projection

Among patients with known outcomes, RLD on the first radiograph was associated with death (AUROC 0.72, 95% CI 0.57–0.86; 17 deaths among 86 patients), similar to age (0.73), and a cross-validated model of RLD and age reached 0.76 Table 2 and Figure 5. RLD was not associated with ICU admission (0.56, 0.45–0.67) or intubation (0.55). The radiographic projection, however, was a strong predictor of ICU admission: AP projection alone gave an AUROC of 0.74 (0.66–0.82), and a cross-validated model using only projection reached 0.72. ICU admission occurred in 88% of patients first imaged AP and 79% of those

imaged AP supine, but in 35% of those imaged PA. The same pattern was present within the single-centre Hannover subset, where 67% of patients imaged AP supine but only 12% of those imaged PA were admitted to the ICU (projection AUROC 0.79 vs. 0.56 for RLD). Projection also influenced the image measure itself: RLD differed between projections (Kruskal–Wallis p = 0.014), and radiologist extent scores were higher for AP (4.5) and AP supine (6.1) than for PA images (3.2).

Table 2. Association of First-Radiograph Measures with Outcomes (AUROC with 95% Bootstrap CI; Cross-Validated Logistic Models without CI)

Predictor	ICU Admission (n = 116–118; 72–73 Events)	Intubation (n = 75–77; 45–47 Events)	Death (n = 65–87; 16–18 Events)
Relative lung density	0.56 (0.45–0.67)	0.55 (0.41–0.68)	0.72 (0.57–0.86)
Age	0.60 (0.43–0.77)	0.63 (0.49–0.76)	0.73 (0.57–0.88)
AP projection	0.74 (0.66–0.82)	0.62 (0.50–0.73)	0.58 (0.45–0.70)
Supine projection	0.63 (0.54–0.71)	0.55 (0.45–0.65)	0.57 (0.45–0.70)
CV model: projection only	0.72	0.51	0.45
CV model: RLD + projection	0.72	0.53	0.66
CV model: RLD + age	0.51	0.59	0.76

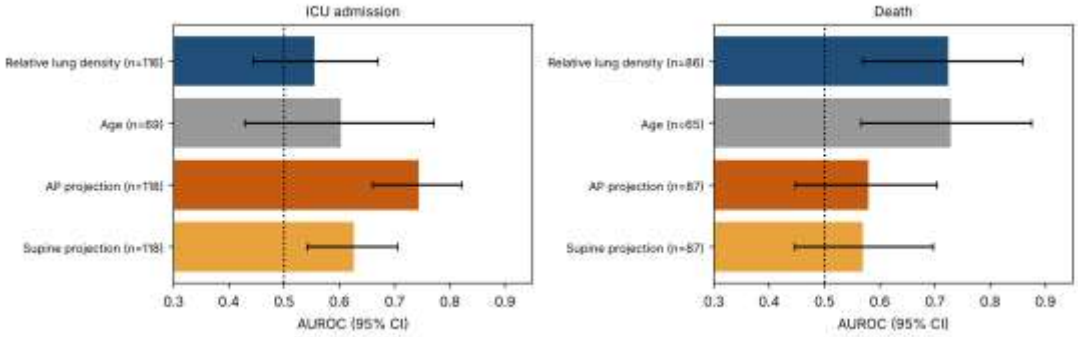

Figure 5. AUROC (95% CI) of Relative Lung Density, Age and Projection on the First Radiograph for ICU Admission (Left) and Death (Right). The Projection, a Property of How and Where the Image Was Acquired, Predicts ICU Admission Better Than the Lung Measure

Figure 6 follows a patient from the Hannover subset with 21 supine radiographs during an ICU stay that ended in death. RLD remained high (0.88–1.06) throughout, but the automatic masks covered only a small, varying part of the lungs, and the images were dominated by tubes, lines and electrodes. Day-to-day changes in RLD therefore reflected positioning and segmentation as much as disease.

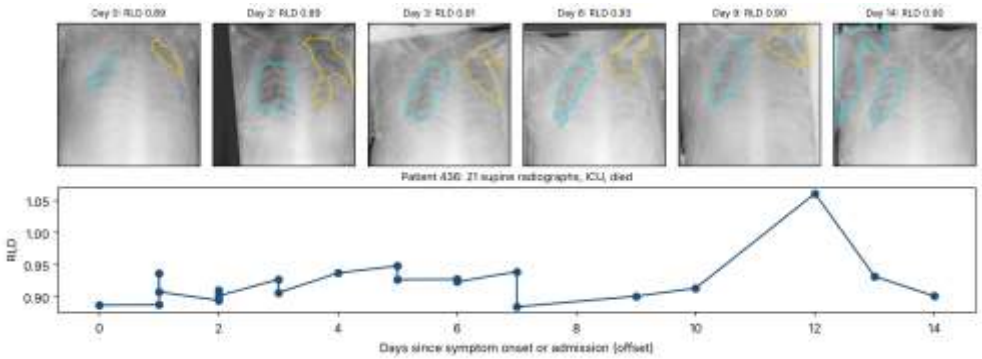

Figure 6. Serial Supine Radiographs of One ICU Patient (Hannover Subset) with Automatic Lung Masks (Top) and Relative Lung Density over Time (Bottom).

3.4 Discussion

This study evaluated a transparent measure of pneumonia severity on real COVID-19 radiographs. Relative lung density, a simple ratio that requires no training on COVID-19 data, correlated moderately with expert severity scores ($\rho \approx 0.6$), and a small zone model improved this only slightly. This is lower than the correlation reported for deep networks trained on the same scores [6], but it was obtained without fitting to those scores except for the choice of normalisation and is fully interpretable. The prominence of the middle zones agrees with the peripheral and mid-to-lower distribution of COVID-19 opacities [2], whereas lower-zone measurements are confounded by the diaphragm and heart.

The segmentation analysis shows why such measures must be validated in severe disease. A network trained on largely normal lungs outlines aerated lung, not the anatomical lung, and therefore excludes the consolidated regions that determine severity. This effect was most pronounced in native ICU radiographs, where a quarter of images had almost no recognised lung. Severity measures built on such masks underestimate disease exactly in the sickest patients and fluctuate with positioning, as the serial case illustrates.

The most important finding concerns confounding. In this collection, the projection predicted ICU admission better than any lung measure, and the same was true within a single hospital. This is expected clinically, since critically ill patients are imaged supine at the bedside, but it means that a model trained to predict ICU admission or intubation from such images can achieve apparently good performance by recognising AP projection, bedside equipment or hospital-specific markers rather than lung disease [9], [10]. Outcome labels in the collection also describe the whole illness, so an ICU radiograph may have been taken after, not before, the outcome. These issues are consistent with the high risk of bias found in reviews of COVID-19 prediction models [7], [8]. Prognostic models from imaging should therefore be trained and evaluated within projection strata or with projection as an explicit covariate, should use images taken before the outcome, and should be validated on consecutive patients from the intended setting [21].

For the management of viral pneumonia, these results support automated density measures as an adjunct for documenting and monitoring disease extent in comparable images, for example serial PA radiographs of ambulatory patients, but not as stand-alone prognostic tools in mixed collections. Their association with mortality, similar to that of age, deserves evaluation in prospective cohorts with standardised acquisition.

The study has limitations. The collection is heterogeneous, with images from publications that may be cropped, annotated or selected for illustrative value; only 93 images had severity scores, almost all PA; and outcomes were missing for most patients and are recorded at the patient level without timing. The density normalisation was selected on the scored images. The lungVAE masks are themselves model outputs and not a manual reference. Finally, the small numbers of deaths and the overlap of scored and outcome subsets limit the precision of prognostic estimates.

4. CONCLUSION

On real chest radiographs from a public COVID-19 collection, an interpretable relative lung density computed within U-Net lung masks correlated moderately with radiologist severity scores and was associated with death to a similar degree as age. A segmentation model trained on another dataset, however, excluded consolidated lung and failed in a quarter of native ICU images, and the radiographic projection alone predicted ICU admission better than any lung measure. Automated severity scoring can support the monitoring of pneumonia, but prognostic use requires segmentation validated in severe disease, images acquired before the outcome and explicit control of acquisition factors such as projection and care setting.

Author Contribution Statement

Name of Author	C	M	So	Va	Fo	I	R	D	O	E	Vi	Su	P	Fu
Astanov Shavkatbek	✓			✓	✓		✓	✓	✓	✓	✓	✓		✓
Chaulagain Dipak	✓	✓	✓	✓	✓			✓		✓		✓		✓

Orozbaeva Zhyldyzkan		✓	✓	✓	✓	✓	✓	✓	✓		✓			✓

C : **C**onceptualization
M : **M**ethodology
So : **So**ftware
Va : **Va**lidation
Fo : **Fo**rmal analysis
I : **I**nvestigation
R : **R**esources
D : **D**ata Curation
O : Writing - **O**riginal Draft
E : Writing - Review & **E**diting
Vi : **Vi**sualization
Su : **Su**pervision
P : **P**roject administration
Fu : **Fu**nding acquisition

Acknowledgments

The authors thank J. P. Cohen and contributors for the COVID-19 image data collection and severity annotations, the Hannover Medical School for releasing its radiographs under an open licence, and the U.S. National Library of Medicine for the Montgomery County dataset, and the researchers whose works have been cited in this study.

Funding Information

This research has received no external funding.

Conflict of Interest Statement

No conflict of interest.

Informed Consent

Not Applicable. The study used only publicly available, anonymised images and metadata.

Ethical Approval

Not Applicable. The study is a secondary analysis of publicly available, anonymised data and involved no human participants.

Data Availability

This study uses the public COVID-19 image data collection [12], the Hannover Medical School image repository [13] and the NLM Montgomery County chest X-ray set [15]. Radiographs reproduced in the figures are from the CC BY 3.0-licensed Hannover subset. No new datasets were created. The analysis code is available from the corresponding author on reasonable request.

Use of Generative AI

Generative AI tools were not used to generate the scientific content, data, analyses or results of this study. Any AI-assisted language editing was reviewed and revised by the authors, who take full responsibility for the content of this article.

REFERENCES

[1] G. D. Rubin et al., "The role of chest imaging in patient management during the COVID-19 pandemic: A multinational consensus statement from the Fleischner Society," Radiology, vol. 296, no. 1, pp. 172–180, 2020. doi.org/10.1148/radiol.2020201365

[2] H. Y. F. Wong et al., "Frequency and distribution of chest radiographic findings in patients positive for COVID-19," Radiology, vol. 296, no. 2, pp. E72–E78, 2020. doi.org/10.1148/radiol.2020201160

[3] A. Borghesi and R. Maroldi, "COVID-19 outbreak in Italy: Experimental chest X-ray scoring system for quantifying and monitoring disease progression," La Radiologia Medica, vol. 125, no. 5, pp. 509–513, 2020. doi.org/10.1007/s11547-020-01200-3

[4] D. Toussie et al., "Clinical and chest radiography features determine patient outcomes in young and middle-aged adults with COVID-19," Radiology, vol. 297, no. 1, pp. E197–E206, 2020. doi.org/10.1148/radiol.2020201754

[5] M. A. Warren et al., "Severity scoring of lung oedema on the chest radiograph is associated with clinical outcomes in ARDS," Thorax, vol. 73, no. 9, pp. 840–846, 2018. doi.org/10.1136/thoraxjnl-2017-211280

[6] J. P. Cohen et al., "Predicting COVID-19 pneumonia severity on chest X-ray with deep learning," Cureus, vol. 12, no. 7, Art. no. e9448, 2020. doi.org/10.7759/cureus.9448

[7] L. Wynants et al., "Prediction models for diagnosis and prognosis of covid-19: Systematic review and critical appraisal," BMJ, vol. 369, Art. no. m1328, 2020. doi.org/10.1136/bmj.m1328

[8] M. Roberts et al., "Common pitfalls and recommendations for using machine learning to detect and prognosticate for COVID-19 using chest radiographs and CT scans," Nature Machine Intelligence, vol. 3, no. 3, pp. 199–217, 2021. doi.org/10.1038/s42256-021-00307-0

[9] A. J. DeGrave, J. D. Janizek, and S.-I. Lee, "AI for radiographic COVID-19 detection selects shortcuts over signal," Nature Machine Intelligence, vol. 3, no. 7, pp. 610–619, 2021. doi.org/10.1038/s42256-021-00338-7

[10] J. R. Zech, M. A. Badgeley, M. Liu, A. B. Costa, J. J. Titano, and E. K. Oermann, "Variable generalization performance of a deep learning model to detect pneumonia in chest radiographs: A cross-sectional study," PLoS Medicine, vol. 15, no. 11, Art. no. e1002683, 2018. doi.org/10.1371/journal.pmed.1002683

[11] J. P. Cohen, P. Morrison, L. Dao, K. Roth, T. Q. Duong, and M. Ghassemi, "COVID-19 image data collection: Prospective predictions are the future," Machine Learning for Biomedical Imaging, vol. 1, Art. no. 002, 2020. doi.org/10.59275/j.melba.2020-48g7

[12] J. P. Cohen et al., "covid-chestxray-dataset," GitHub repository. Accessed: Oct. 2026. github.com/ieee8023/covid-chestxray-dataset

[13] Institute for Diagnostic and Interventional Radiology, Hannover Medical School, "covid-19-image-repository" (released under CC BY 3.0), GitHub repository. Accessed: Oct. 2026. github.com/ml-workgroup/covid-19-image-repository

[14] O. Ronneberger, P. Fischer, and T. Brox, "U-Net: Convolutional networks for biomedical image segmentation," in Medical Image Computing and Computer-Assisted Intervention – MICCAI 2015, LNCS vol. 9351, Springer, 2015, pp. 234–241. doi.org/10.1007/978-3-319-24574-4_28

[15] S. Jaeger, S. Candemir, S. Antani, Y.-X. J. Wáng, P.-X. Lu, and G. Thoma, "Two public chest X-ray datasets for computer-aided screening of pulmonary diseases," Quantitative Imaging in Medicine and Surgery, vol. 4, no. 6, pp. 475–477, 2014. doi.org/10.3978/j.issn.2223-4292.2014.11.20

[16] S. Candemir et al., "Lung segmentation in chest radiographs using anatomical atlases with nonrigid registration," IEEE Transactions on Medical Imaging, vol. 33, no. 2, pp. 577–590, 2014. doi.org/10.1109/TMI.2013.2290491

[17] R. Selvan et al., "Lung segmentation from chest X-rays using variational data imputation," in ICML Workshop on The Art of Learning with Missing Values (Artemiss), 2020. doi.org/10.48550/arXiv.2005.10052

[18] J. M. Bland and D. G. Altman, "Statistical methods for assessing agreement between two methods of clinical measurement," The Lancet, vol. 327, no. 8476, pp. 307–310, 1986. doi.org/10.1016/S0140-6736(86)90837-8

[19] F. Pedregosa et al., "Scikit-learn: Machine learning in Python," Journal of Machine Learning Research, vol. 12, pp. 2825–2830, 2011. jmlr.org/papers/v12/pedregosa11a.html

[20] A. Paszke et al., "PyTorch: An imperative style, high-performance deep learning library," in Advances in Neural Information Processing Systems (NeurIPS), vol. 32, 2019, pp. 8024–8035. doi.org/10.48550/arXiv.1912.01703

[21] G. S. Collins, J. B. Reitsma, D. G. Altman, and K. G. M. Moons, "Transparent reporting of a multivariable prediction model for individual prognosis or diagnosis (TRIPOD): The TRIPOD statement," BMJ, vol. 350, Art. no. g7594, 2015. doi.org/10.1136/bmj.g7594

How to Cite: Astanov Shavkatbek, Chaulagain Dipak, Orozbaeva Zhyldyzkan. (2026). Quantifying COVID-19 pneumonia severity on chest radiographs: Automated lung density, radiologist scores, clinical outcomes and the confounding role of image acquisition. Journal of Prevention, Diagnosis and Management of Human Diseases (JPDMHD), 6(2), 33-42. https://doi.org/10.55529/jpdmhd.62.33.42

BIOGRAPHIES OF AUTHORS

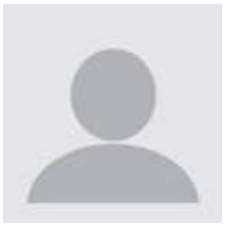	**Astanov Shavkatbek**, works as a lecturer in the Department of Clinical Disciplines at Jalal-Abad International University, Manas, Kyrgyzstan, and serves as corresponding author for this paper. The study quantifies COVID-19 pneumonia severity on chest radiographs and demonstrates how acquisition factors, notably anteroposterior versus posteroanterior projection, can confound the prediction of clinical outcomes. Email: astanovshavkat697@gmail.com
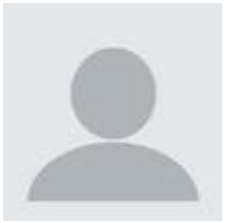	**Chaulagain Dipak**, occupies an associate professorship in the Department of Clinical Disciplines at Jalal-Abad International University. Chaulagain Dipak contributed as co-author to this investigation, which set an automated, segmentation-based lung-density measure beside radiologist extent and opacity scores in patients with COVID-19 and related it to intensive-care admission and death.
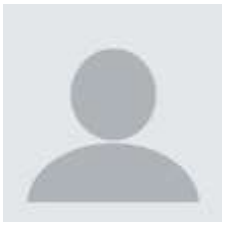	**Orozbaeva Zhyldyzkan**, is associate professor in the Department of Natural and Humanities Disciplines, Jalal-Abad International University, Kyrgyzstan. Working from a department outside the clinical faculties, Orozbaeva Zhyldyzkan took part as third author in this analysis of a public, multi-source collection of COVID-19 chest images drawn from several hospitals and published case reports.